Investigation on the mechanical behavior of planetary roller screw with the effects of external loads and machining errors

Xing Du, Bingkui Chen*, Zhengding Zheng

The State Key Laboratory of Mechanical Transmissions, Chongqing University, Chongqing 400030, China

Abstract:

Planetary roller screws are the key mechanical components used in linear motion and could be subjected to radial and axial loads in application. However, the effect of radial force on load distribution and fatigue life has not been considered in previous studies. This paper exactly establishes the connection between planetary roller screw internal deformation and external load, the load distribution models are based on equivalent contact deformation and contact force, and amended by considering radial loads, machining errors and corrections under tension-compression or tension-tension working state. Then, the numerical calculations point out the influences of configurations, external forces, machining accuracy and corrections on load capacity, deformation coefficient and fatigue life of planetary roller screw. The results reveal that when the planetary roller screw is applied with radial force, the contact loads reduces periodically with the growth of thread number. Moreover, with the increase of machining errors, the deformation coefficients and contact forces change dramatically at a certain load. After proper modification, the fatigue life and the uniformity of load capacity are remarkably improved. The proposed approach and analytical results show load characteristics of planetary roller screw and thereby proffer the fundamental insights needed to guide the design, installation and use of planetary roller screw.

Keywords: planetary roller screw; load capacity; deformation coefficient; fatigue life; machining error

1. Introduction

Planetary roller screw mechanisms (PRSM) are considered as the key component of linear motion in engineering applications. With the ever-increasing development of electric aircrafts, automobile, robots, and other fields, the heavy load, high accuracy, high power-to-weight ratio, extreme temperature and long lifetime are strongly demanding for the PRSM. These requirements lead to greatly large contact stress, high sliding velocity, and instantaneous temperature in the PRSM, which are easy to surpass the endurance limit. In such situations, the accuracy, stability, durability and reliability of the PRSM will be a significant challenge. Therefore, it is extremely important to accurately calculate the load distribution and predict fatigue life of the PRSM.

Over the past decades, many excellent works have been done in the literature, which mainly target the geometry, kinematics, load capacity, friction, lubrication, dynamics, thermal and fatigue life [1-9]. Sandu et al. [1], [2] proposed an efficient method for analyzing thread geometry and predicting contact ellipses. Jones and Velinsky [3] analyzed the accurate kinematics of the roller migration because of pitch deviation. Abevi et al. [4] presented a fundamental approach considering the axial resilience and bending flexibility of the roller, and predicted the load capacity and static stiffness of the roller in the different configurations. Ma et al. [5] researched the contact characteristic with the tangential friction and normal pressure, and derived the relative velocities at the screw-roller and roller-nut interfaces. The results revealed that sliding

contact and rolling contact were the main contact methods for screw-roller and roller-nut interface, respectively. Xie et al. [6] proposed the mixed-lubrication model, and found that the speed and surface roughness had significant influences on film thickness, friction coefficient and contact-area ratio. Jones et al. [7] presented the accurate dynamic equations with viscous friction based on Lagrange's Method, and showed that the dependence of slip velocity on the lead and contact angle of the screw. Qiao et al. [8] analyzed the thermal characteristics of the PRSM under mutative working conditions, and found that the speed, grease and external load played significant roles in temperature rise level and thermal failure. Lemor [9] proposed a basic method to predict the fatigue life of the PRSM.

For the investigation of the mechanical behavior of the PRSM, how to exactly establish the connection between the internal deformation and the external load is a significant problem. Yang et al. [10] analyzed the load distribution law based on Hertz theory. Ma et al. [11] established a load capacity model with errors, and revealed that the load distribution was remarkably affected by the axial force, contact angle, helix angle, etc. Zhang et al. [12], [13] found the load distribution was greatly sensitive to pitch deviation and proposed an improvement method to make load distribution uniform. Abevi et al. [14] presented the contact deformations under different working state by numerical analysis, and founded that the machining errors and position errors had great influences on the number of effective contacts.

All of the above studies have helped researchers have a better understanding of the mechanical behavior over threads of the PRSM. However, the mechanical behavior of PRSM is affected by many factors, such as radial loads, machining errors, corrections and so on. Existing models barely have an overall consideration of these factors. Their works mentioned above aimed at analyzing the load distribution and fatigue life only subjected to axial loads. Recently, many scholars paid more attention to the ball screw considering radial loads, which was partially similar with the PRSM. Zhen and An [15] established the analytical model of ball screw to investigate the contact stress and fatigue life, and showed that the sensitivity of the load distribution and fatigue life with the dimension errors of balls. Zhao et al. [16] analyzed the influence of turning torque and geometric errors on the ball screw performance, and revealed that the different effects of ball's accuracy and axial load on the ball screw of load distribution, position precision and fatigue life. However, the contact deformation of the PRSM has not been adequately performed by the method of ball screw, mainly because of the accumulative axial deformations of threads.

In this study, an explicit mechanical model readily and rapidly available to analyze the load distribution and predict the fatigue life of a PRSM is built with respect to external loads (axial load and radial load), machining errors, configurations and corrections. Firstly, the axial force of each roller is estimated by the equivalent contact load and deformation. Then, the deformation compatibility equation is amended by considering external loads and machining errors under the tension-compression (T-C) or tension-tension (T-T) working state. Further, the load capacity, deformation coefficient and fatigue life are analyzed due to the effects of axial loads, radial loads and machining errors. Finally, based on load coefficient of the PRSM, the corrections

of roller are presented in order to improve the uniformity of load capacity and increase lifetime.

2. Mechanical model

2.1. Initial assumptions

Fig. 1 shows a scheme of the PRSM. For the purpose to obtain a practical analytical model and reduce ambiguity, the necessary hypotheses should be made:

1) All contact deformations are considered as elastic deformations, which only occur in the contact area and conform to the Hertz contact theory;
2) Centrifugal force and gyroscopic moment are negligible due to the low rotation speed of the screw;
3) The top roller is 1#, and the sequence number increases clockwise;
4) The separation angle of any roller *i*# with respect to 1# roller is φ_i, which could be calculated by:

$$\varphi_i = \frac{2\pi(i-1)}{n} \quad (i = 1, 2, ..., n) \tag{1}$$

where n is the total number of rollers.

2.2. Contact load and deformation analysis

2.2.1. Equivalent contact load and deformation

As shown in Fig. 2, when the PRSM is subjected to radial load, the radial contact deformation at different position angle is generated. Fig. 2 shows the solid circle represents the initial position of the nut, and the dotted circle denotes the new position of the nut under external loads. According to Ref. [6], [11], for the purpose to obtain the load capacity, the axial load of each roller is given as an input parameter and the contact deformations and contact forces are solved. However, when the PRSM is subjected to both axial and radial loads, the axial load of each roller is not the same. Furthermore, it's also extremely difficult to calculate the normal contact deformations of all threads in accordance with geometry relationship. Hence, in order to get the axial load of each roller, it is firstly assumed that the axial deformation $\delta a_{(i,j)}$ of all threads are identical, and the radial deformation of *i*# roller can be described by[15]:

$$\delta_{r(i,j)} = \delta_r \cos\psi_i \tag{2}$$

ψ_i is the position angle of *i*# roller and can be written by:

$$\psi_i = \varphi_i + \theta \tag{3}$$

by varying θ, the radial deformation of any thread can be known.

Therefore, the equivalent contact deformation $\delta^E_{n(i,j)}$ of screw-roller and nut-roller

interface in the normal direction can be calculated by:

$$\delta_{n(i,j)}^{E} = \delta_{a(i,j)} \sin\beta / \cos\lambda + \delta_{r(i,j)} \cos\beta \cos\varphi_i \tag{4}$$

Where β is the contact angle; λ is the helix angle of roller.

And then, the equivalent contact load $Q_{n(i,j)}^{E}$ in the normal direction can be obtained according to the load-deformation relationship of the PRSM:

$$Q_{n(i,j)}^{E} = \gamma (K\delta_{n(i,j)}^{E})^{3/2} \quad \begin{cases} \gamma = 1, \delta_{n(i,j)}^{E} > 0 \\ \gamma = 0, \delta_{n(i,j)}^{E} \le 0 \end{cases} \tag{5}$$

where the index $\gamma = 1$ denotes that the thread couple are contacting, while $\gamma = 0$ represents that the thread couple are not in contact. The symbol K is total contact stiffness coefficient in the screw-roller and nut-roller interface, which depends on the design parameters of the PRSM. It can be determined by:

$$K = \frac{1}{K_{rn} + K_{rs}} \tag{6}$$

where K_{rs} and K_{rn} are the contact stiffness of screw-roller interface and nut-roller interface, respectively, and which are expressed as[6]:

$$\begin{cases} K_{rs} = \dfrac{K_{es}}{\pi m_{as}} \sqrt[3]{\dfrac{(3E)^2 \sum \rho_s}{4}} \\ K_{rn} = \dfrac{K_{en}}{\pi m_{an}} \sqrt[3]{\dfrac{(3E)^2 \sum \rho_n}{4}} \end{cases} \tag{7}$$

where K_{es} and K_{en} are the complete elliptic integral of the first kind of screw-roller and roller-nut interface, respectively; m_{as} and m_{an} are the major semi-axis coefficients of the contact ellipse of the screw-roller and roller-nut interface, respectively; E represents the effective Young moduli; $\sum \rho_{\mathrm{s}}$ and $\sum \rho_{\mathrm{n}}$ are the curvature sum of screw-roller and roller-nut interface, respectively.

According to Eqs. (1) ~ (7), the equilibrium equations of equivalent contact load of the PRSM with axial load and radial load are obtained by:

$$\begin{cases} F_r - \sum_{i=1}^{n} \sum_{j=1}^{t} Q_{n(i,j)}^{E} \sin\beta \cos\lambda = 0 \\ F_a - \sum_{i=1}^{n} \sum_{j=1}^{t} Q_{n(i,j)}^{E} \cos\beta \cos\varphi_i = 0 \end{cases} \tag{8}$$

where F_r and F_a are the radial load and axial load on the PRSM, respectively; t is the total thread number of any roller.

Hence, the axial contact load of any roller can be calculated by:

$$F_{ai} = \sum_{j=1}^{t} Q_{n(i,j)}^{E} \cos\beta \cos\varphi_i \tag{9}$$

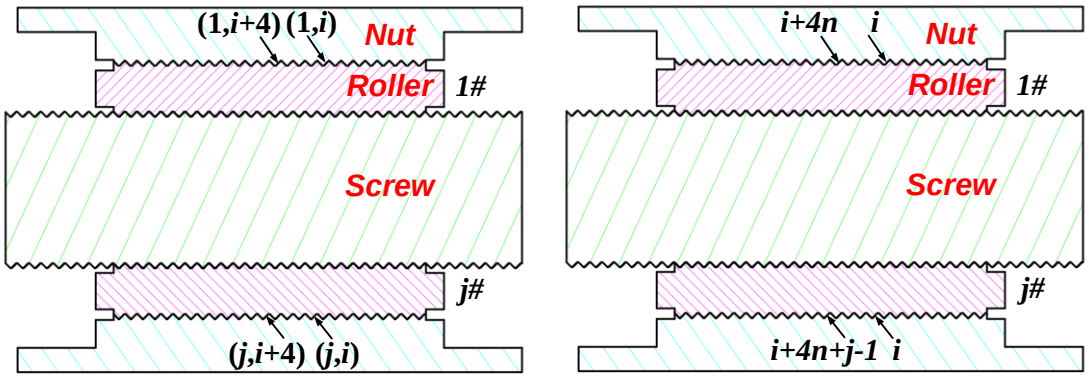

(a) Individual numbering of each roller thread

(b) Roller threads are numbered along the circumference

Fig. 1. Schematic diagram of PRSM

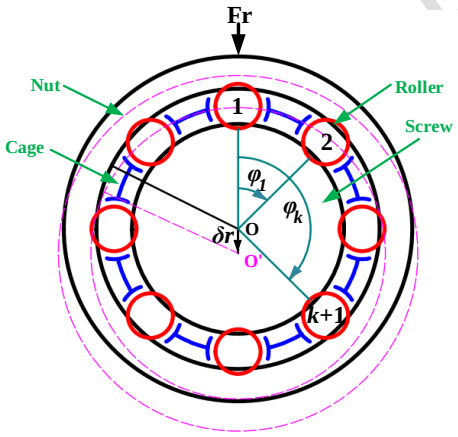

Fig. 2. The diagram of radial deformation

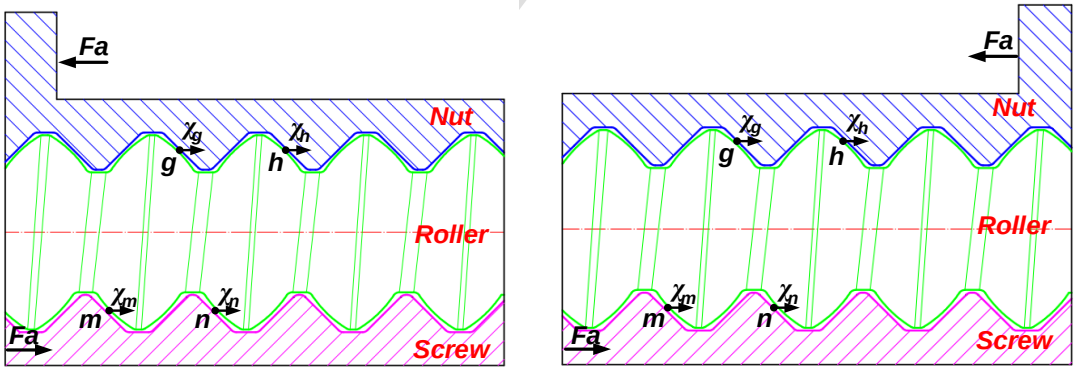

(a) T-C state

(b) T-T state

Fig. 3. The diagram of axial deformation with errors

2.2.2. Theoretical contact load and deformation in T-C

According to the equilibrium condition and Fig. 3(a), the axial load under the T-C working state can be calculated by:

$$F_{S(i,j)} = F_{N(i,j)} = F_{ai} - \sum_{i=1}^{n}\sum_{k=1}^{j-1} Q_{n(i,k)} \sin\beta\cos\lambda \tag{10}$$

Where $F_{S(i,j)}$ and $F_{N(i,j)}$ are the axial force of the screw and nut, respectively. $Q_{n(i,j)}$ is

the normal contact force, which complies with the following conditions:

$$\begin{cases} F_r - \sum_{i=1}^{n}\sum_{j=1}^{t} Q_{n(i,j)} \sin\beta\cos\lambda = 0 \\ F_a - \sum_{i=1}^{n}\sum_{j=1}^{t} Q_{n(i,j)} \cos\beta\cos\varphi_j = 0 \end{cases} \tag{11}$$

And then, the axial deformation considering the machining errors in the screw-roller interface at the contact points *m* and *n* can be expressed by:

$$\chi_{S(i,j)} = \chi_m - \chi_n = \frac{1}{\sin\beta\cos\lambda}(\delta_{S(i,j-1)} - \delta_{S(i,j)}) - (\varepsilon_{S(i,j-1)} - \varepsilon_{S(i,j)}) \tag{12}$$

where $\delta_{S(i,j)}$ and $\delta_{S(i,j-1)}$ are the Hertz contact deformation of j^{th} and j-1^{th} thread in screw-roller interface, respectively. $\varepsilon_{S(i,j)}$ and $\varepsilon_{S(i,j-1)}$ are the axial machining errors of j^{th} and j-1^{th} thread in the screw-roller interface, respectively. Similarly, that of the nut-roller interface can be written as:

$$\chi_{N(i,j)} = \chi_g - \chi_h = \frac{1}{\sin\beta\cos\lambda}(\delta_{N(i,j-1)} - \delta_{N(i,j)}) - (\varepsilon_{N(i,j-1)} - \varepsilon_{N(i,j)}) \tag{13}$$

where $\delta_{N(i,j)}$ and $\delta_{N(i,j-1)}$ are the Hertz contact deformation of j^{th} and j-1^{th} thread in nut-roller interface, respectively. $\varepsilon_{N(i,j)}$ and $\varepsilon_{N(i,j-1)}$ are the axial machining errors of j^{th} and j-1^{th} thread in the roller-nut interface, respectively

Combined with Eqs. (12) and (13), the total axial deformation with machining errors can be calculated by:

$$\chi_{(i,j)} = (\chi_m + \chi_g) - (\chi_n + \chi_h) = \frac{1}{\sin\beta\cos\lambda}(\delta_{n(i,j-1)} - \delta_{n(i,j)}) - (\varepsilon_{n(i,j-1)} - \varepsilon_{n(i,j)}) \tag{14}$$

where $\delta_{n(i,j)}$ and $\delta_{n(i,j-1)}$ denote the total Hertz contact deformation of j^{th} and j-1^{th} thread of $i^{\#}$ roller, respectively. $\varepsilon_{n(i,j)}$ and $\varepsilon_{n(i,j-1)}$ represent the total axial machining errors of j^{th} and j-1^{th} thread of $i^{\#}$ roller, respectively.

$$\begin{cases} \delta_{n(i,j)} = \delta_{S(i,j)} + \delta_{N(i,j)},\ \delta_{n(i,j-1)} = \delta_{S(i,j-1)} + \delta_{N(i,j-1)} \\ \varepsilon_{n(i,j)} = \varepsilon_{S(i,j)} + \varepsilon_{N(i,j)},\ \varepsilon_{n(i,j-1)} = \varepsilon_{S(i,j-1)} + \varepsilon_{N(i,j-1)} \end{cases} \tag{15}$$

Furthermore, the axial deformation in the screw-roller and the nut-roller interface can also be calculated by:

$$\begin{cases} \chi_{S(i,j)} = \dfrac{F_{S(i,j)}p}{2E_S A_S},\ A_S = \pi R_S^2 \\ \chi_{N(i,j)} = \dfrac{F_{N(i,j)}p}{2E_N A_N},\ A_N = \pi(R_{oN}^2 - R_N^2) \end{cases} \tag{16}$$

where p is the pitch; A_S and A_N are the cross-sectional areas of screw and nut, respectively; R_S and R_N are the nominal radius of screw and nut, respectively. R_{oN} is the external radius of nut.

According to Eq. (16), the total axial deformation can also be calculated by:

$$\chi_{(i,j)} = \frac{F_{N(i,j)} p(A_S + A_N)}{2E_S A_S A_N} \tag{17}$$

Based on Eqs. (14) and (17), the recursive equation with machining errors can be obtained by:

$$Q_{n(i,j-1)}^{2/3} - Q_{n(i,j)}^{2/3} - \frac{(\varepsilon_{(i,j-1)} - \varepsilon_{(i,j)}) \sin\beta\cos\lambda}{K_{rs} + K_{rn}} = \frac{\sum_{i=1}^{n}\sum_{k=j}^{t} Q_{n(i,k)} \sin^2\beta\cos^2\lambda\, p(A_s + A_n)}{2E_s A_s A_n (K_{rs} + K_{rn})} \tag{18}$$

2.2.3. Theoretical contact load and deformation in T-T

According to the equilibrium condition and Fig. 3(b), the axial load under T-T working state can be revised by:

$$\begin{cases} F_{S(i,j)} = F_a - \sum_{i=1}^{n}\sum_{k=1}^{j-1} Q_{n(i,k)} \sin\beta\cos\lambda \\ F_{N(i,j)} = \sum_{i=1}^{n}\sum_{k=1}^{j} Q_{n(i,k)} \sin\beta\cos\lambda \end{cases} \tag{19}$$

where $Q_{n(i,j)}$ complies with Eq. (11).

According to Fig. 3(b), the axial deformation in the screw-roller interface can also be expressed by Eq. (12), while that of the nut-roller interface can be amended as:

$$\chi_{N(i,j)} = \chi_g - \chi_h = \frac{1}{\sin\beta\cos\lambda}(\delta_{N(i,j)} - \delta_{N(i,j-1)}) - (\varepsilon_{N(i,j)} - \varepsilon_{N(i,j-1)}) \tag{20}$$

Combined with Eqs. (12) and (20), the total axial deformation with machining errors can be calculated by:

$$\chi_{(i,j)} = \chi_{S(i,j)} - \chi_{N(i,j)} = \frac{1}{\sin\beta\cos\lambda}(\delta_{n(i,j-1)} - \delta_{n(i,j)}) - (\varepsilon_{n(i,j-1)} - \varepsilon_{n(i,j)}) \tag{21}$$

With Eqs. (16) and (19), the total axial deformation can also be calculated by:

$$\chi_{(i,j)} = -\frac{F_a p}{2EA_N} + \frac{\left[\sum_{i=1}^{n}\sum_{k=j}^{t} Q_{n(i,k)}(A_S + A_N) - Q_{n(i,j)} A_S\right] p \sin\beta\cos\lambda}{2EA_S A_N} \tag{22}$$

According to Eqs. (21) and (22), the recursive equation with errors in T-T can be obtained as:

$$\begin{aligned} &Q_{n(i,j-1)}^{2/3} - Q_{n(i,j)}^{2/3} - \frac{(\varepsilon_{(i,j-1)} - \varepsilon_{(i,j)}) \sin\beta\cos\lambda}{K_{rs} + K_{rn}} + \frac{F_a p \sin\beta\cos\lambda}{2E_s A_n (K_{rs} + K_{rn})} = \\ &\frac{\left[\sum_{i=1}^{n}\sum_{k=j}^{t} Q_{n(i,k)}(A_s + A_n) - Q_{n(i,j)} A_s\right] p \sin^2\beta\cos^2\lambda}{2E_s A_s A_n (K_{rs} + K_{rn})} \end{aligned} \tag{23}$$

2.3. Deformation coefficient and load coefficient

2.3.1 Deformation coefficient

Comparing with the contact loads without errors, the contact loads with errors can be either larger or smaller. The contact deformations also are changed with the variation of the machining errors. Deformation errors are difficult to compensate due to changing deformations[16]. Hence, in order to evaluate contact deformation of the PRSM with machining errors, the deformation coefficient is introduced and expressed as:

$$\tau_{(i,j)} = \frac{\delta^0_{n(i,j)}}{\delta_{n(i,j)}} \tag{24}$$

where $\delta^0_{n(i,j)}$ and $\delta_{n(i,j)}$ denote the normal contact deformation without error and with error, respectively.

If Eq. (5) is substituted into Eq. (24), $\tau_{(i,j)}$ is represented as:

$$\tau_{(i,j)} = \left(\frac{Q^0_{n(i,j)}}{Q_{n(i,j)}} \right)^{\frac{2}{3}} \tag{25}$$

where $Q^0_{n(i,j)}$ and $Q_{n(i,j)}$ are the normal contact load without errors and with errors, respectively.

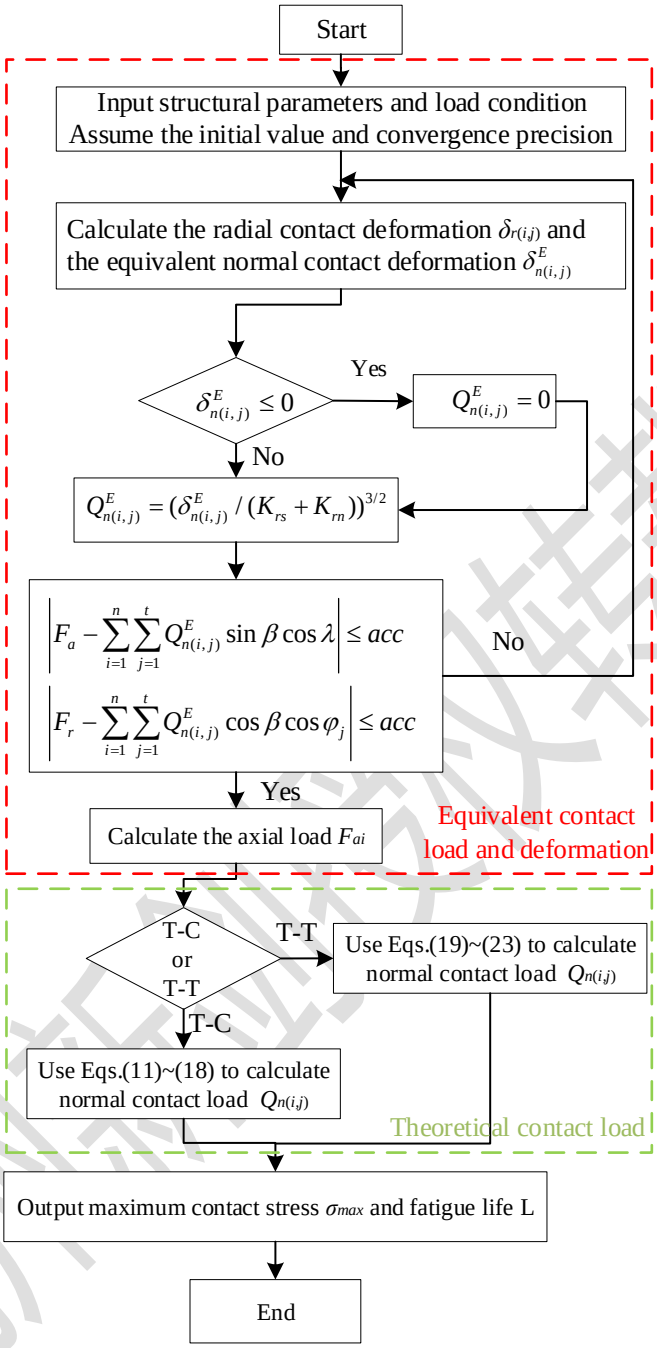

Fig. 4. Calculation flow of static model

Furthermore, the range value v_i, the difference between the maximum and the minimum deformation coefficient in $i^{\#}$ roller, is introduced to present the fluctuation of deformation coefficient, which is calculated by:

$$\upsilon_i = \max(\tau_{(i,j)}) - \min(\tau_{(i,j)}) \tag{26}$$

2.3.2 load coefficient

In order to intuitively investigate the load capacity, the load coefficient κ, defined as the ratio of the contact load to the minimum contact load and expressed by Eq. (27), is introduced to evaluate the variation of contact force of the PRSM. The load

coefficient varies with the contact load variation. Thus, the coefficient directly reveals the nonuniformity of load capacity.

$$\kappa_{(i,j)} = \frac{Q^0_{n(i,j)}}{\min(Q^0_{n(i,j)})} \tag{27}$$

2.4. Fatigue life analysis

Fatigue life is one of the most important performance of the PRSM in practical applications. In this part, the fatigue life of the PRSM is discussed based on the previous analysis. According to the stress-life approach, the lifetime of the PRSM is determined by contact stress and rotate speed. Commonly, the basis for formulating fatigue life of the PRSM is the maximum contact stress, which can be obtained by:

$$\sigma_{\max} = \frac{3Q_{n\max}}{2ab} \tag{28}$$

where Q_{nmax} denotes the maximum contact force in normal direction, the major semi-axis a and minor semi-axis b of the contact ellipse can be calculated by[17]:

$$a = m_a \sqrt[3]{\frac{3Q_{n\max}E}{2\sum\rho}}, b = m_b \sqrt[3]{\frac{3Q_{n\max}E}{2\sum\rho}} \tag{29}$$

where m_b is expressed as:

$$m_b = \sqrt[3]{\frac{2K(e)}{\pi(1-e^2)}} \tag{30}$$

And then, the fatigue curve of material can be written as:

$$N_H = k_\sigma^m N_0 \tag{31}$$

where N_0 is the circulation base of the material. k_σ represents the stress ratio between contact fatigue limit σ_0 and maximum contact stress σ_{max} and is written by:

$$k_\sigma = \frac{\sigma_0}{\sigma_{\max}} \tag{32}$$

Furthermore, the absolute rotating speed of the roller around the screw can be expressed as[18]:

$$\omega_R = \frac{\omega_S k_m (k_m + 2)}{2(k_m + 1)} \tag{33}$$

where k_m denotes the ratio between screw nominal diameter d_S and roller nominal diameter d_R and is expressed by:

$$k_m = \frac{d_S}{d_R} \tag{34}$$

Therefore, the fatigue life in hour is estimated by[15]:

$$L = \frac{N_H(k_m+1)}{60\omega_s k_m(k_m+2)} \tag{35}$$

Based on the above analysis, the entire calculation process for the fatigue life and contact forces of the planetary roller screw is shown in Fig. 4.

3. Numerical examples and discussion

In order to verify the validity and accuracy of the proposed model, some numerical examples are presented by the specific parameters. These examples cover contact loads, fatigue life and deformation coefficients considering the effects of configurations, external loads, machining errors and corrections. Table 1 and Table 2 show the detail parameters of the PRSM. In this example, there are 24 threads in a roller and 192 threads in all rollers.

Table 1.

Design parameters of the PRSM

	Roller		**Screw**		**Nut**	
Parameters (Unit)	Symbol	Values	Symbol	Values	Symbol	Values
Nominal radius (mm)	R_r	4	R_s	12	R_n	20
Contact angle (◦)	β	45	β	45	β	45
Starts	S_r	1	S_s	5	S_n	5
Helix angle (°)	λ_r	4.55	λ_S	1.52	λ_n	0.91
Pitch (mm)	P_r	2	P_s	2	P_n	2
Number	n_r	8	n_s	1	n_n	1
External radius (mm)	/	/	/	/	R_{on}	27.5

Table 2.

Material parameters of the PRSM

Parameters (Unit)	**Symbols**	**Values**	**Parameters (Unit)**	**Symbols**	**Values**
Young moduli (Pa)	E	2.12×10^{11}	Poisson's ratio	μ	0.29
Circulation base	N_0	2.5×10^{8}	hardness of parts	HRC	62
contact fatigue limit (N/mm^2)	σ_0	2450	point contact index of the steel	m	6

3.1. Effects of external loads

Fig. 5 depicts the load capacity under the T-T and T-C working state when machining errors are zero, and the PRSM is assumed that under the next two conditions: 1) the axial load F_a = 30kN and the radial load F_r = 3kN; 2) the axial load F_a = 30kN and the radial load F_r = 0kN. In Fig. 5, the load capacity without radial load is represented by the dotted line, while that with radial load is denoted by the full line. Square, circle, upper triangle, lower triangle and diamond markers are the load capacity of 1#, 2# and 8#, 3# and 7#, 4# and 6#, 5# roller with radial load, respectively.

As shown in Fig. 5(a), it can be observed that the load capacity curves of all rollers

are superimposed when the PRSM is not subjected to radial force. With the increase of the thread number, the contact loads monotonically decrease, but the slopes of the curves increase. This is notably consistent with the observation from Ref. [13]. Nevertheless, the load distribution curves vary when the PRSM is applied with radial force. In a lead, the contact forces of the 8 pairs of thread contact couple are no longer the same, but are either larger or smaller. Moreover, for the position angle from 0° to 180°, the contact loads from 1# roller to 5# roller gradually decrease with the decrease of radial load. For the position angle from 180° to 360°, the contact loads from $5^{\#}$ roller to $1^{\#}$ roller gradually increase with the growth of radial load. This is mainly due to the fact that increasing or decreasing radial load of rollers makes the Hertz contact deformation larger or smaller at different position angle, which results in the variation of contact loads. Moreover, the load capacity curves of 3# and 7# rollers with radial force are the same as that of any roller without radial force, and they may also be considered as the mean of all rollers with radial force. And then, Fig. 5(b) shows the load capacity under the T-T state. Comparing Fig. 5(b) with Fig. 5(a), the contact forces do not always decrease with the growth of thread number, but first decrease and then increase. This phenomenon occurs mainly because under the T-T state, the axial load is applied near the first thread of roller in screw-roller side and the last thread in the roller-nut side, so that the load distribution can become slightly uniform.

Fig. 6 shows the contact loads of 1# roller in the cycling process. For the T-C and T-T case in Fig. 6, it can be notably found that under the same thread, the contact loads of the PRSM without radial force don't change in the cycling process while those vary periodically under radial load. The changing trend of contact force is similar with the ball screw of Ref.[15]. Moreover, the contact forces under the same position angle reduce obviously with the increase of thread number in Fig. 6(a) and Fig. 6(b), while that in Fig. 6(c) and Fig. 6(d) decrease at first and then increase. That is well confirmed by Fig. 5. Because the changing tendency of load capacity is similar with each roller, this part takes $1^{\#}$ roller as an example.

3.1.1 Effects of the axial loads

Fig. 7 represents the variation of load capacity against thread number under the same radial load and the different axial load. As the T-C case shown in Fig. 7(a), the PRSM with different axial load shows the different load distribution curves. The contact forces over threads are undoubtedly increased with the growth of axial loads. Meanwhile, with the increase of thread number, the contact force reduces periodically. And then, Fig. 7(b) shows the load capacity for the T-T case. We can find that the peak value of contact force and the downward trend of the load distribution curve under the T-T state is smaller than Fig. 7(a) under the same external load. Furthermore, the contact forces decrease at first and then increase periodically. Thus, it can be concluded that the load capacity becomes more even under the T-T state, and the uniformity of that cuts down with increase of axial load.

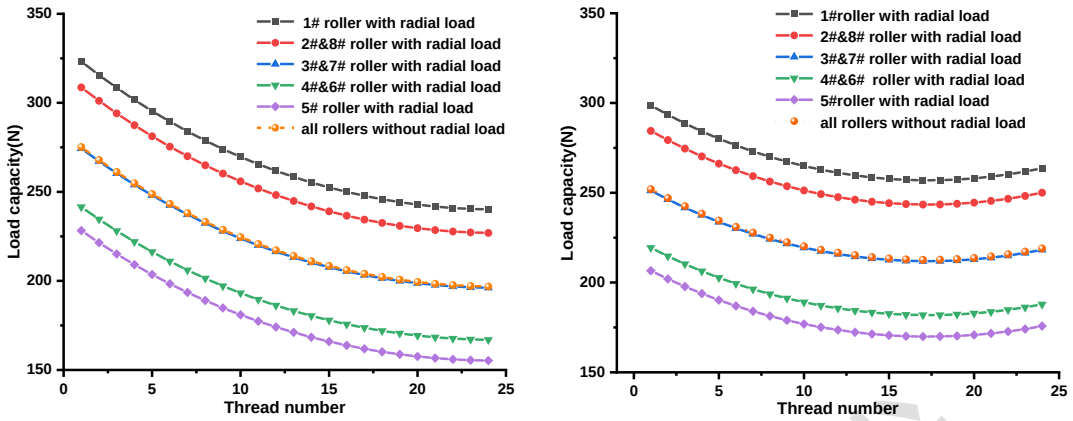

(a) T-C state (b)T-T state

Fig. 5. Load capacity in different configurations

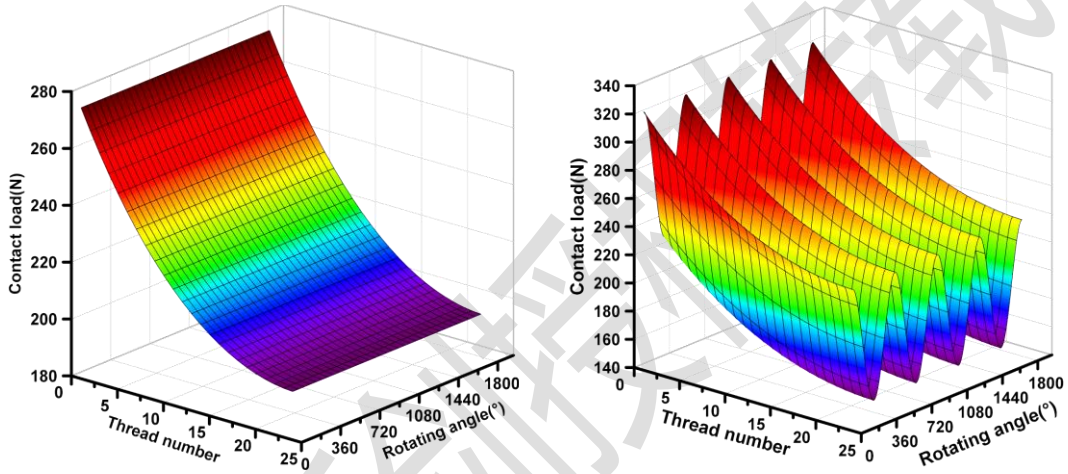

(a) No radial load under the T-C state (b) With radial loads under the T-C state

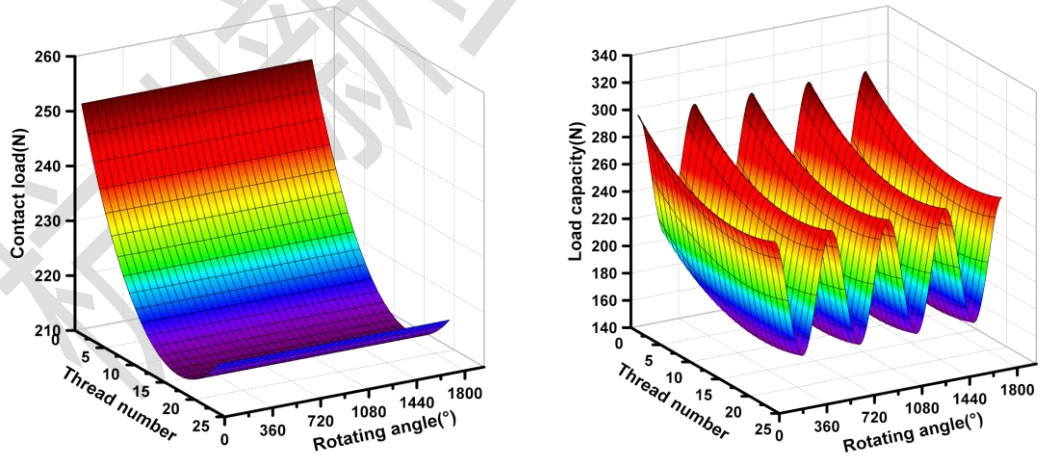

(c) No radial load under the T-T state (d) With radial loads under the T-T state

Fig. 6. Load capacity of 1# roller in cycling in different configurations and external loads.

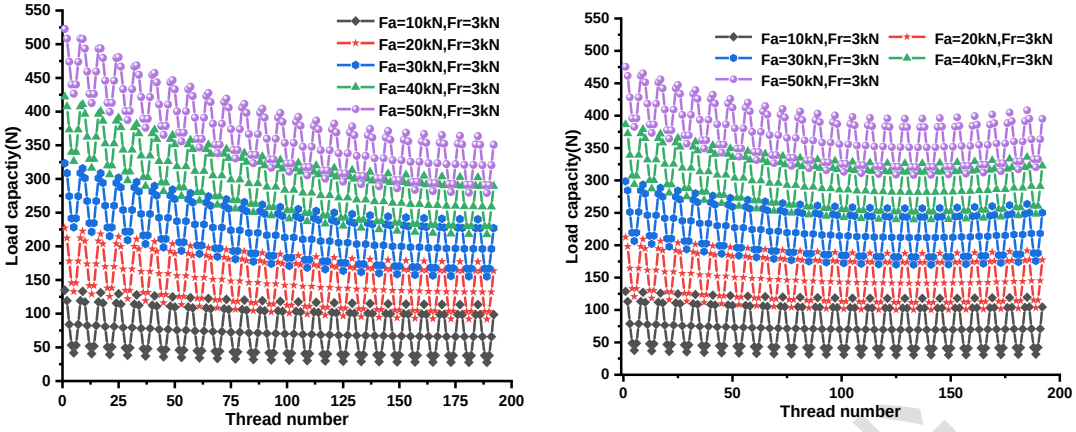

(a) T-C state (b) T-T state

Fig. 7. Load distribution in different axial loads and configurations.

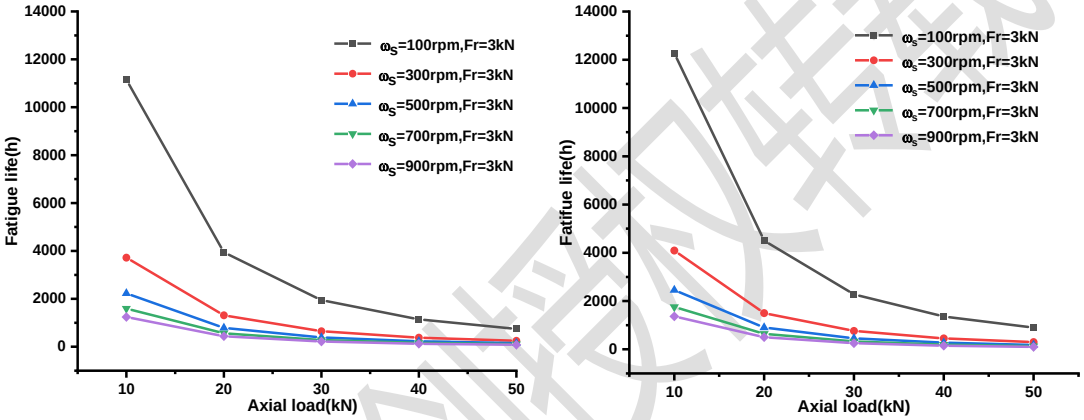

(a) T-C state (b) T-T state

Fig. 8. Fatigue life in different axial loads, rotating speeds and configurations

Fig. 8 shows the fatigue life against the axial load under the different rotate speed and the same radial load. Fig. 8(a) shows the fatigue life under the T-C state. As the rotate speed is 100rpm, with the increase of the axial load, the fatigue life is reduced rapidly first and then slowly. However, when the rotate speed is higher than 100rpm, the fatigue life sharply decreases under the same external loads and slowly decreases with the increase of axial load. In addition, when the axial load is bigger than 30kN, the fatigue life has little variation against the rotate speed. Therefore, the fatigue life under the low axial load is more sensitive to rotate speed than that under the large axial load. This can also be obtained by Eq. (35). And then, the fatigue life under the T-T state is shown in Fig. 8(b), and the result is similar with Fig. 8(a). The discrepancy is that the lifetime slightly increases. This is mainly because that the maximum contact load is smaller under the T-T state than that under the T-C state. This can be confirmed by Fig. 7. Hence, the fatigue life is susceptible to rotate speed under the low axial load.

3.1.2 Effects of the radial loads

Fig. 9 shows the load capacity against the thread number under the different radial load and the same axial load. As shown in Fig. 9, the influence of thread number on the load capacity is similar with that of Fig. 7 when the axial load is 20kN. Moreover, it

can be evidently observed that with larger radial load, the load capacity curves have more severe fluctuation under the same axial load.

Fig. 10 indicates the dependence of fatigue life on the radial load and rotate speed. It can be obviously seen that when the PRSM with lower speed can have longer the fatigue life, especially the speed is less than 100rpm. In addition, the fatigue life significantly decreases with the increase of radial load. The main reason is why the maximum contact load remarkably increases with the growth of the radial load. The maximum contact stress can also be evidently increased and thereby the fatigue life can be visibly decreased. Therefore, during the design, installation and use of the PRSM, radial forces should be reduced as much as possible, which coincides with the proposed application of the SKF or ROLLVIS SWISS product catalog[19],[20].

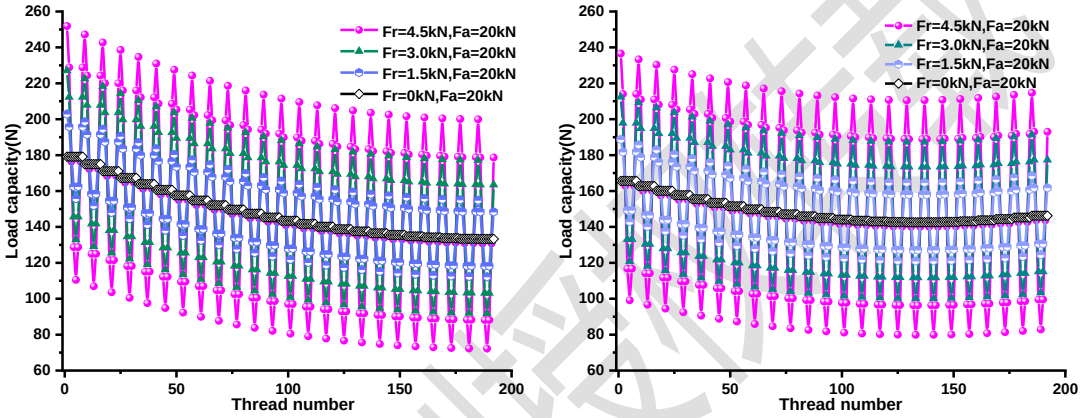

(a) T-C state (b) T-T state

Fig. 9. Load distribution in different radial loads and configurations.

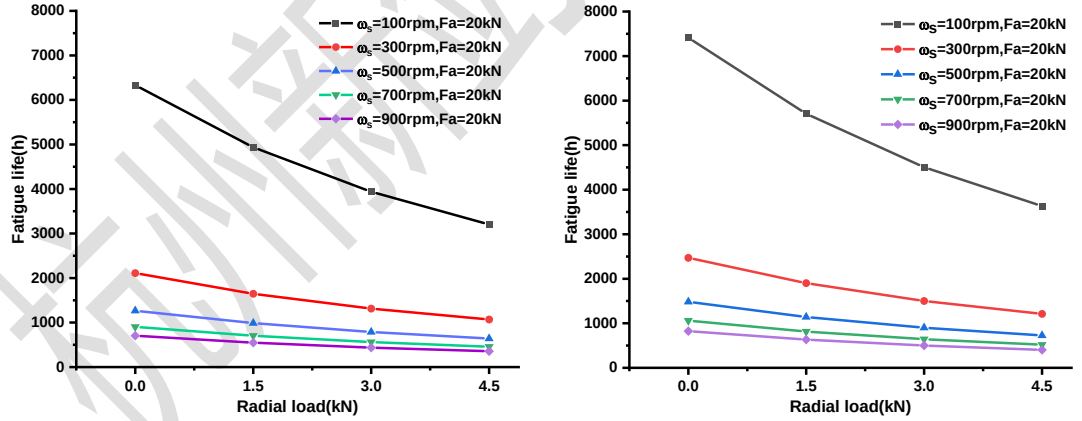

(a) T-C state (b) T-T state

Fig. 10. Fatigue life in different radial loads, rotate speeds and configurations.

3.2. Effects of machining errors

In fact, the machining errors of the PRSM are inevitable and can be considered as a kind of random errors. Among the machining errors, the pitch deviation is the most influential on the mechanical performance[12]. Therefore, in this paper, the load capacity, fatigue life and deformation coefficient are mainly analyzed due to the effects of pitch errors.

3.2.1 Effect of one thread with error

Fig. 11 shows the load capacity against the thread number with 2μm and -2μm in 4th thread of 1# roller. It's obviously seen that when the error is negative in 4th thread, the contact force of the corresponding thread notably decreases, and those of the other threads slightly increase. In contrast, when the error of the 4th thread is positive, its contact force remarkably increases, and those of the remaining threads slightly decrease. This is mainly because that the positive error makes the axial clearance between thread couple smaller so that the contact deformation and contact load of the corresponding thread couple becomes bigger. On the contrary, the clearance is increased due to negative error and the contact deformation and contact force reduce.

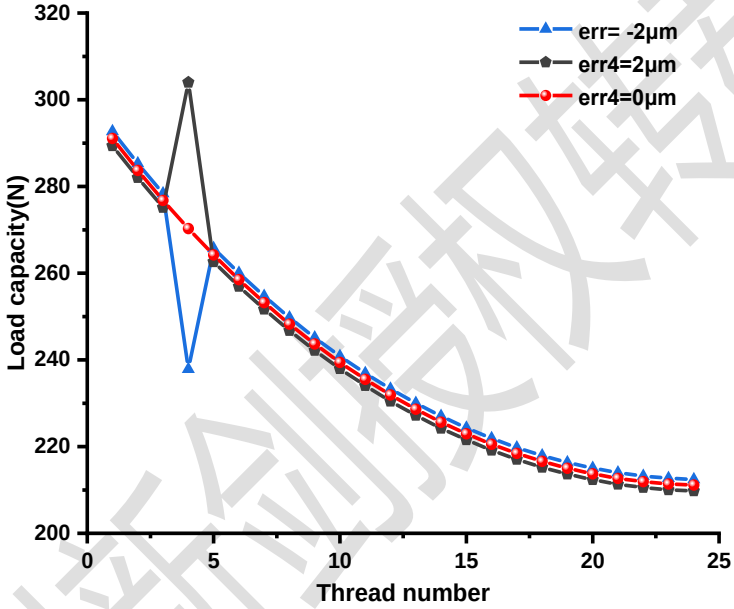

Fig. 11. Load capacity with the errors of 2μm and -2μm in 4th thread of 1$^{\#}$ roller

3.2.2 Effects of all threads with errors

In order to intuitively and accurately track the effects of machining errors, all threads have random ptich errors. The error curves are shown in Fig. 12, the error ranges are ±2μm and ±4μm, respectively. These errors are generated by the random function in MATLAB.

Fig. 13 shows the variation of load capacity in the thread number under the different pitch errors and same external loads. As shown in Fig. 13, the errors have critical influences on the load capacity. It can be obviously seen that the load capacity curves of the PRSM with larger pitch errors fluctuate more severely. The main reason is why the bigger the pitch error, the greater or smaller the axial clearance, and the larger or smaller the contact deformation and contact force. Therefore, in the design process, the pitch errors should be minimized without interference.

In order to deeply investigate the effects of machining errors, the deformation coefficient under the T-C state against the thread number and axial load under the

different pitch errors and the same radial load of 1kN. As shown in Fig. 14, both the axial loads and pitch errors evidently change the deformation coefficient. Obviously, comparing the deformation coefficient of ±2μm with that of ±4μm for given axial loads, there is a larger fluctuation of deformation coefficient under ±4μm. This is mainly because that the larger the pitch errors, the bigger the variation of contact force and deformation. This is well confirmed by Fig. 13. In addition, with the growth of axial load, the deformation coefficient reduces rapidly at first and then slowly for ±4μm case. It can be observed that the deformation coefficient under the low axial load is more sensitive to machining errors than that under the large axial load. Therefore, the PRSM can properly reduce the machining accuracy under heavy loads.

The fatigue life under the T-C state against machining errors shown in Fig. 15 and Fig. 16. Fig. 15 depicts the fatigue life against the axial load and accuracy under the same radial load of 1kN and the same feed rate of 300 rpm. As shown in Fig. 15, for given a specific accuracy, the PRSM with the lager axial load can possess a shorter lifetime than that of the PRSM with smaller axial load. This agrees well with Fig. 8(a). Furthermore, the fatigue life with a stable axial load has a clear downward trend with the reduction of the machining accuracy. This is mainly accounts for the lower the machining accuracy, the more uneven the distribution, and the maximum contact force increases as Fig. 13 illustrates. And then, Fig. 16 represents the variation of fatigue life in radial load and machining accuracy under the same axial load of 30kN and rotate speed of 300rpm. It can be interestingly noted that when the machining accuracy is stable, the fatigue life tends to remarkably decrease with the growth of radial load. This is consistent with Fig. 10. Furthermore, the change of fatigue life with radial force and machining accuracy is almost the same as that of the axial force.

Table 3

Roller's pitch error with different accuracy (unit μm)

Accuracy	A0	A1	A2	A3	A4	A5
Dimension error	0.5	1	2	3	4	5

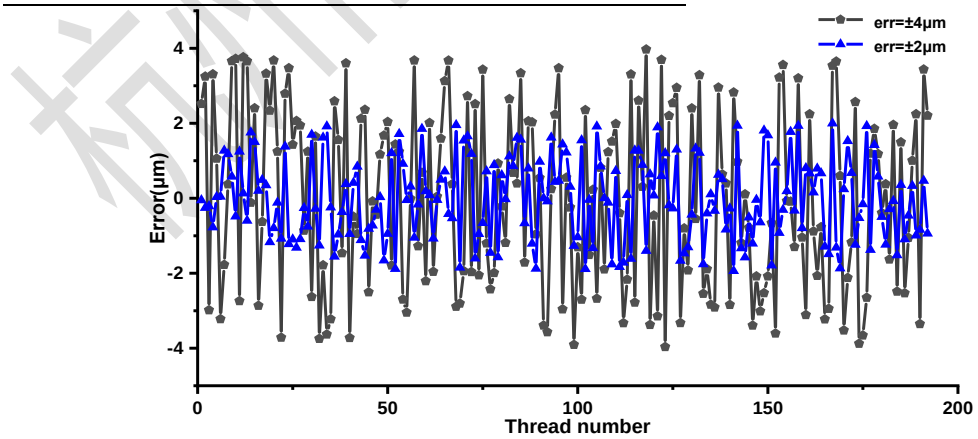

Fig. 12. Random pitch errors of all roller threads

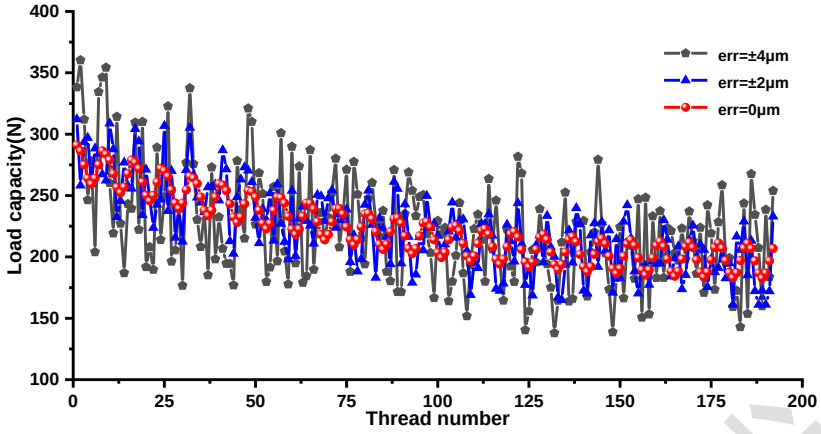

(a) T-C state

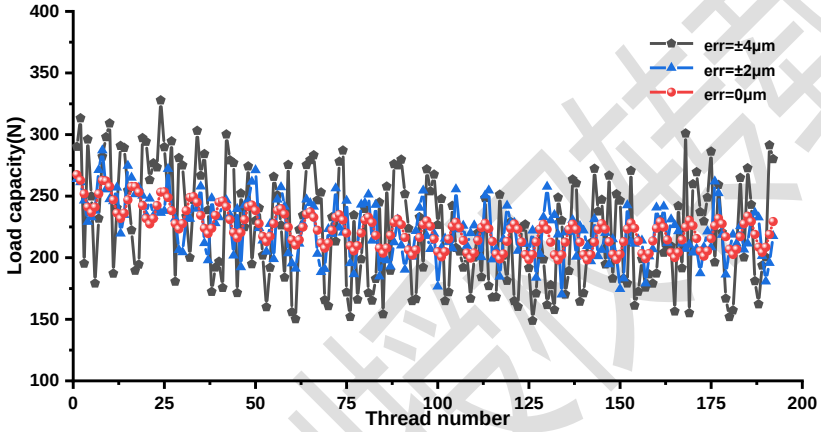

(b) T-T state

Fig. 13. Load distribution with random errors

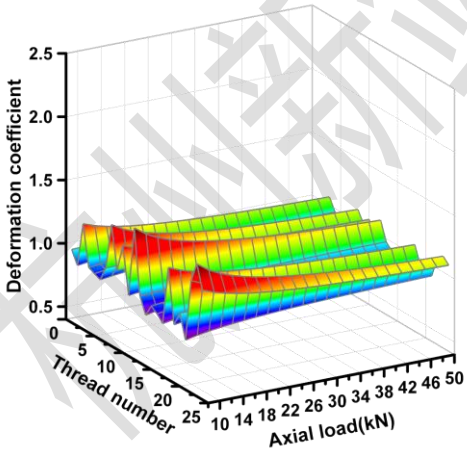

(a)1# roller with the pitch error of 2.0μm

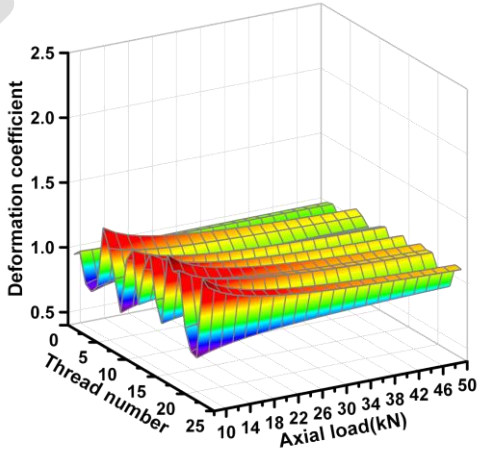

(b)3# roller with the pitch error of 2.0μm

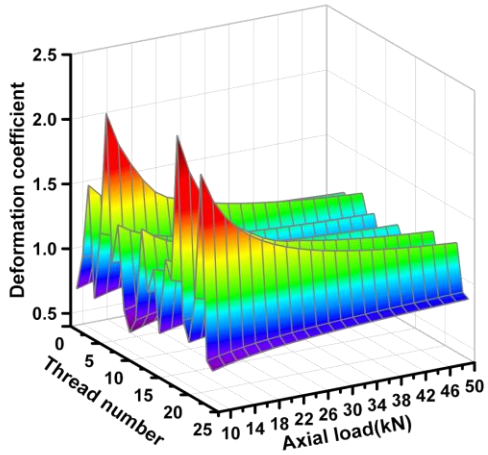

(c)1# roller with the pitch error of 4.0μm

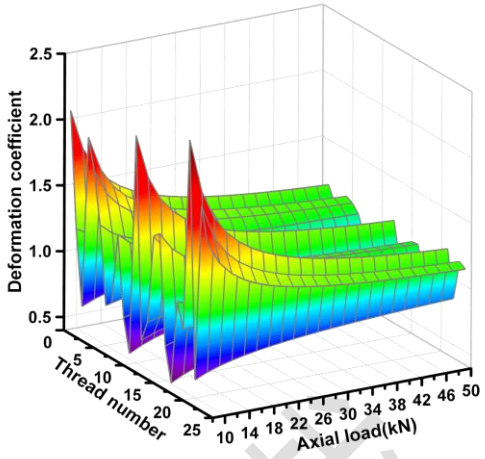

(d)3# roller with the pitch error of 4.0μm

Fig. 14. Deformation coefficient in different pitch errors and axial loads

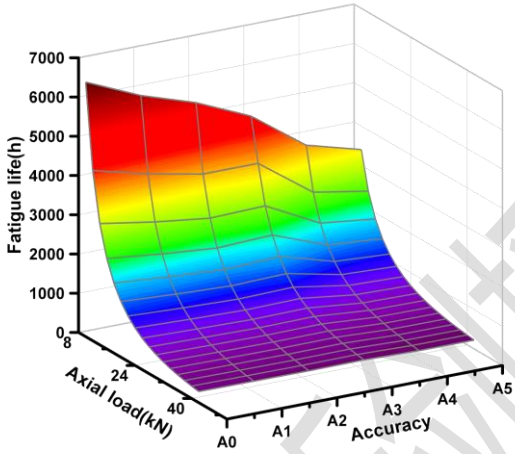

Fig. 15. Fatigue life in different machining accuracy and axial loads

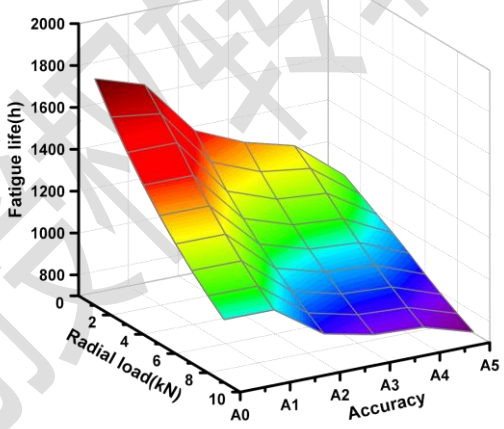

Fig. 16. Fatigue life with machining accuracy and radial loads

3.3. Effects of form correction of rollers

From Section 3.2 we can find that when the threads have errors, the contact forces of the corresponding threads increase or decrease. Therefore, in order to achieve uniform load distribution and improve lifetime, the thread forms of rollers are modified. The modification is based on the load coefficient. According to Eq. (18), the recursive equation with corrections can be revised by:

$$Q_{n(i,j-1)}^{2/3} - Q_{n(i,j)}^{2/3} - \frac{1}{K_{rs}+K_{rn}}[c(\kappa_{(i,j-1)} - \kappa_{(i,j)})] = \frac{n\sum_{j=i}^{t} Q_{n,ij} \sin^2\beta \cos^2\lambda\, p(A_s + A_n)}{2A_s A_n (K_{rs}+K_{rn})} \tag{36}$$

where c is the modification factor.

As shown in Fig. 17, it indicates that the amount of modification of roller thread under the T-C state is inversely proportional to the load coefficient. It can also be found that the greater the contact load, the larger the amount of modification. Furthermore,

the correction curves of each roller are almost consistent under the same external load.

Interesting, it can be found that the minimum Hertzian contact load increases and the maximum Hertzian contact load decreases after the modification displayed in Fig. 18. This is due to the fact that the accumulative axial deformations can be compensated by the corrections. Compared with the four sets of modification, we can find that with the increase of correction, the uniformity of load capacity curve increases at first and then reduces evidently. In addition, the load capacity curves with 9κ corrections are more uniform than that of other corrections at specific load. As shown in Fig. 18(c), the maximum and minimum contact force of $1^{\#}$ roller with 9κ modification are 239.5N and 235.5N, respectively; while those without modification are 291.1N and 211.1N, respectively. Consequently, the range of contact forces with modification is 95% lower than that without modification. However, as shown in Fig. 19, the load capacity curves of the PRSM shows 9κ correction is immoderate when the load is less than 30kN and is not enough when the load is more than 30kN. In addition, Fig. 20 indicates that the load capacity curves of the PRSM with correction is more uniform than that without correction in extensive range when the axial loads increase or reduce. Therefore, proper modification can effectively improve the load distribution of PRSM to a certain extent.

Fig. 21 shows the variation of fatigue life against the correction under the same external load and rotate speed. In this part, the PRSM is assumed that under the following condition: the axial load Fa = 30kN, and the radial load Fr = 3kN, and rotate speed ω_s = 100rpm, and change the corrections from 0κ to 12κ. It can be seen that the fatigue life of the PRSM increases at first and then decreases with the growth of corrections. Hence, the proper correction is an effective way to increase the fatigue life.

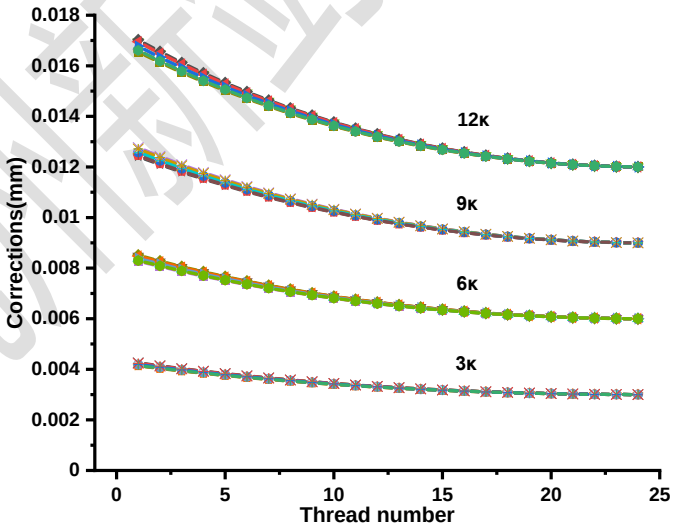

Fig. 17. Correction curves with different modification factors.

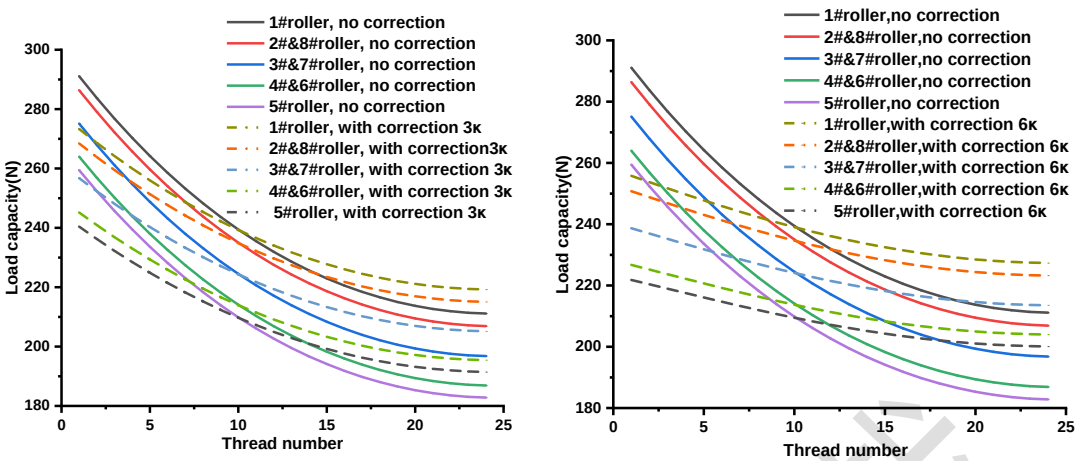

(a) 3κ correction (b) 6κ correction

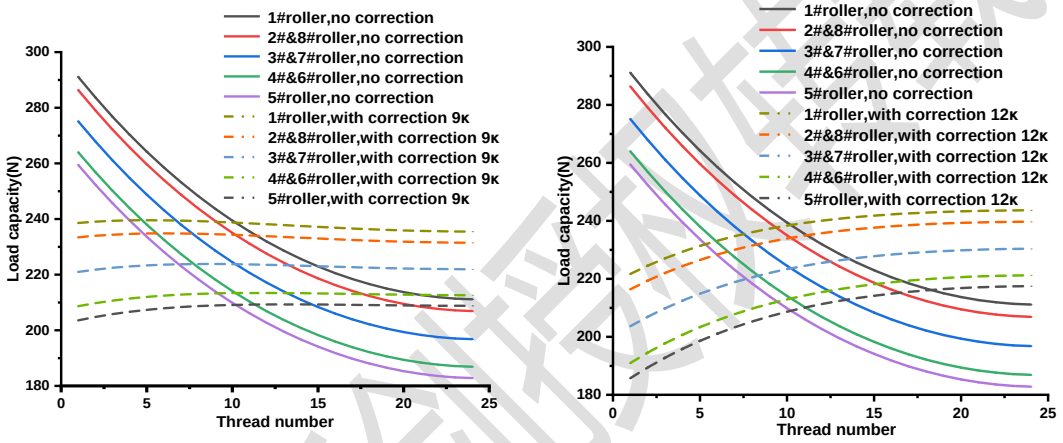

(c) 9κ correction (d) 12κ correction

Fig. 18. Load capacity in different corrections

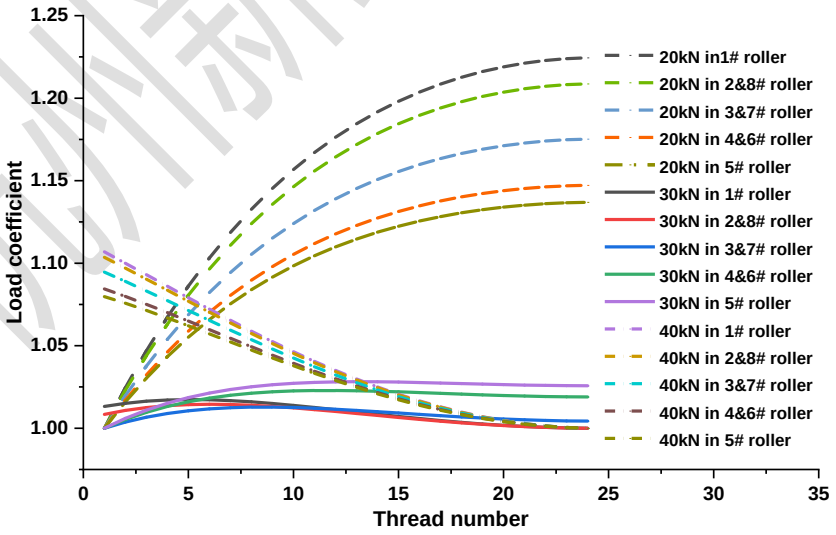

Fig. 19. Load capacity of 9κ correction in different axial loads

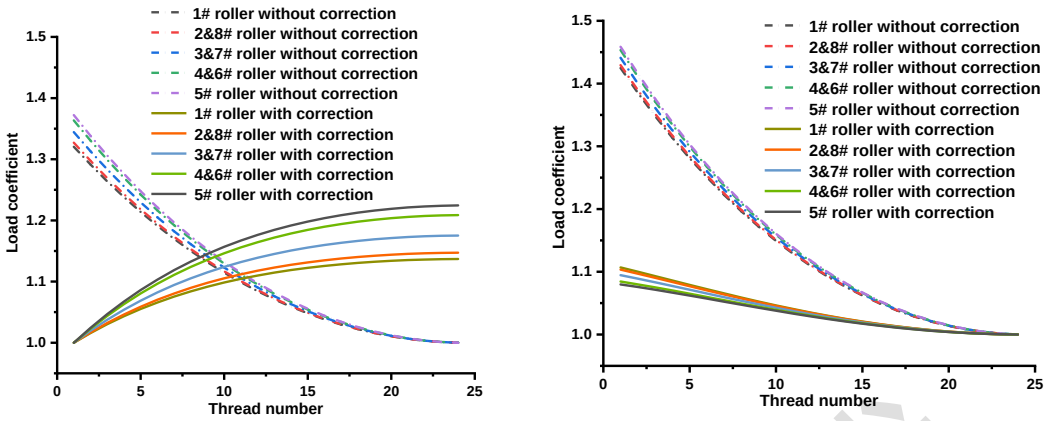

(a) Axial load in 20kN (b) Axial load in 40kN

Fig. 20. Load capacity of 9κ correction in different axial loads and same radial load of 3kN

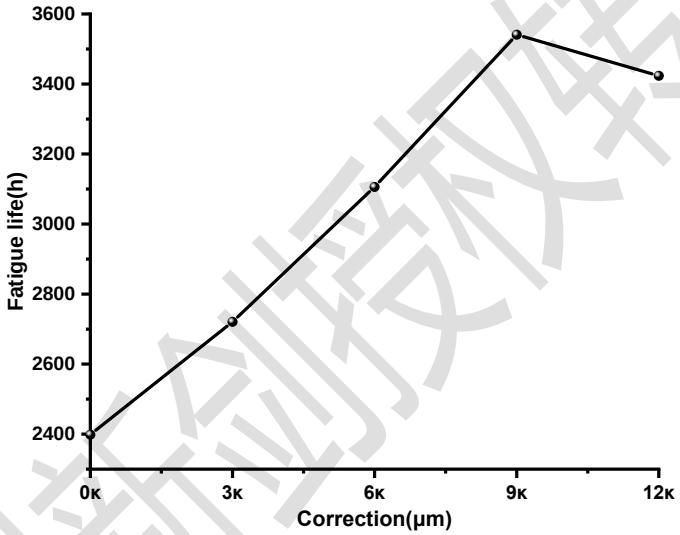

Fig. 21. Fatigue life in different corrections

4. Conclusions

In this paper, the proposed model for investigating the load capacity, deformation coefficient and fatigue life of the PRSM is performed. This model considering radial load makes use of the equivalent method for axial force estimation of individual rollers. Moreover, the effects of radial loads, axial loads, configurations, machining errors or corrections are taken into consideration. In order to verify the validity and accuracy of the proposed model, lots of analysis results are done, and the following conclusions can be obtained:

(1) when the PRSM is applied with axial load and radial load, the load capacity of the PRSM changes periodically. As the axial loads increase, the contact forces and the non-uniformity of load capacity increase, resulting in the lifetime decreasing. In addition, with the growth of radial loads, the load distribution curves oscillate intensely and the fatigue life decreases sharply. Therefore, during the design, installation and use of the PRSM, radial forces should be reduced as much as

possible.

(2) The configurations affect load capacity and fatigue life. Comparing the T-T with the T-C state, the contact force slightly become uniform and the fatigue life slightly increases.

(3) The machining errors have great influences on load capacity, deformation and fatigue life. As the error of a thread is negative, the corresponding thread contact force decrease, but the rest increase. In contrast, the positive error makes contact load of the corresponding thread increase, while the others decrease. Moreover, the deformation coefficient varies dramatically with increasing errors, and decreases rapidly at first and then slowly through increase of axial load. Hence, the load distribution of large axial load isn't particularly sensitive to the effect of machining accuracy. Furthermore, for given an external load, the fatigue life of PRSM has a decrease trend with the decrease of machining accuracy.

(4) The minimum Hertzian contact load remarkably increases and the maximum Hertzian contact load significantly decreases after the roller threads are corrected. Comparing the modified PRSM with the PRSM without modification, the contact forces over threads becomes more even and the fatigue life of PRSM is notably improved.

Acknowledgments

This work was supported by the National Key Research and Development Program of China (Grant No. 2017YFB1300704).

Reference

[1] S. Sandu, et al., An efficient method for analyzing the roller screw thread geometry, Mechanism and Machine Theory, 126 (2018) 243-264.

[2] S. Sandu, et al., Analytical prediction of the geometry of contact ellipses and kinematics in a roller screw versus experimental results, Mechanism and Machine Theory, 131 (2019) 115-136.

[3] M.H. Jones, S.A. Velinsky, Kinematics of Roller Migration in the Planetary Roller Screw Mechanism, Journal of Mechanical Design, 134 (2012).

[4] F. Abevi, et al., Static Load Distribution and Axial Stiffness in a Planetary Roller Screw Mechanism, Journal of Mechanical Design, 138 (2016).

[5] S. Ma, et al., Modelling of static contact with friction of threaded surfaces in a planetary roller screw mechanism, Mechanism and Machine Theory, 139 (2019) 212-236.

[6] Z. Xie, et al., Mixed-lubrication analysis of planetary roller screw, Tribol. Int., 140 (2019) 105883.

[7] M.H. Jones, et al., Dynamics of the Planetary Roller Screw Mechanism, Journal of Mechanisms and Robotics, 8 (2015).

[8] G. Qiao, et al., Thermal characteristics analysis and experimental study of the planetary roller screw mechanism, Applied Thermal Engineering, 149 (2019) 1345-1358.

[9] P.C. Lemor, Mechanical drives combine efficiency and reliability, 69 (1997).

[10] J. Yang, et al., Calculation of load distribution of planetary roller screws and static rigidity, journal of huazhong university of science and technology(natural science edition), 39 (2011) 1-5.

[11] S. Ma, et al., Load distribution of rollers considering errors in planetary roller screw mechanism, Harbin Gongye Daxue Xuebao/journal of Harbin Institute of Technology, 47 (2015) 98-102.
[12] W. Zhang, et al., Load distribution over threads of planetary roller screw mechanism with pitch deviation, Proceedings of the Institution of Mechanical Engineers Part C-Journal of Mechanical Engineering Science, 233 (2019) 4653-4666.
[13] W. Zhang, et al., Load distribution of planetary roller screw mechanism and its improvement approach, Proceedings of the Institution of Mechanical Engineers Part C-Journal of Mechanical Engineering Science, 230 (2016) 3304-3318.
[14] F. Abevi, et al., Static Analysis of an Inverted Planetary Roller Screw Mechanism, Journal of Mechanisms and Robotics, 8 (2016).
[15] N. Zhen, Q. An, Analysis of stress and fatigue life of ball screw with considering the dimension errors of balls, International Journal Of Mechanical Sciences, 137 (2018) 68-76.
[16] J.J. Zhao, et al., Investigation of load distribution and deformations for ball screws with the effects of turning torque and geometric errors, Mechanism And Machine Theory, 141 (2019) 95-116.
[17] K.L. Johnson, Contact mechanics, Cambridge University Press, New York;Cambridge, 1985.
[18] S. Ma, et al., Kinematics of Planetary Roller Screw Mechanism considering Helical Directions of Screw and Roller Threads, Mathematical Problems in Engineering, (2015).
[19] SKF, Roller Screws Catalog, (2018).
[20] ROLLIVIS, Satellite roller screw, (2019).